Optics Communications 452 (2019) 417–421

Contents lists available at ScienceDirect

Optics Communications

journal homepage: www.elsevier.com/locate/optcom

# Cherenkov excited luminescence imaging induced by megavolt X-ray beams in the second near-infrared window

Xiangxi Meng [a,b], Yi Du [c], Ruoxi Wang [c], Ziyuan Li [a], Sihao Zhu [a], Hao Wu [c,*], Changhui Li [a,*], Weiqiang Chen [d], Shuming Nie [e], Qiushi Ren [a], Yanye Lu [f,*]

[a] Department of Biomedical Engineering, College of Engineering, Peking University, Beijing 100871, China
[b] The Wallace H. Coulter Department of Biomedical Engineering, Georgia Institute of Technology & Emory University, Atlanta, GA 30332, USA
[c] Key laboratory of Carcinogenesis and Translational Research (Ministry of Education/Beijing), Department of Radiation Oncology, Peking University Cancer Hospital & Institute, Beijing 100142, China
[d] Institute of Modern Physics, Chinese Academy of Sciences, Key Laboratory of Heavy Ion Radiation Biology and Medicine of Chinese Academy of Sciences, Key Laboratory of Basic Research on Heavy Ion Radiation Application in Medicine, Gansu Province, Lanzhou 730000, China
[e] Department of Biomedical Engineering, University of Illinois at Urbana-Champaign, Urbana, IL 61801, USA
[f] Pattern Recognition Lab, Friedrich-Alexander-University Erlangen–Nuremberg, 91058 Erlangen, Germany

ARTICLE INFO

*Keywords:*
Second near-infrared window
Cherenkov radiation
X-ray
Radiotherapy

ABSTRACT

The Cherenkov radiation induced by megavolt X-ray beams of a medical linear accelerator is highly intense in blue and ultraviolet lights. This poses a challenge for *in vivo* imaging, which favors longer wavelengths. However, using quantum dots with a large Stokes shift, we converted the Cherenkov photons to fluorescent photons in the second near-infrared (NIR-II) window. A system was designed to provide shielding for the NIR-II camera, and high quality NIR-II CELI signal was acquired. The NIR-II CELI of X-ray beams was shown at various depths, and the condition to trigger it was also studied. Animal experiments showed this technique could visualize the delivery of X-ray radiation in mice qualitatively. We concluded that CELI induced by megavolt X-ray beams in the NIR-II window possesses a great potential as a quality control tool in radiotherapy.

## 1. Introduction

Owing to its superior characteristics, the second near-infrared (NIR-II) window has gained intense attention in *in vivo* fluorescence imaging [1,2]. The benefits of this specific spectrum range (1000 nm to 1700 nm) include decreased tissue scattering and low autofluorescence with acceptable low absorption [3]. Over the past years, instrumental development, NIR-II contrast agents, and various pre-clinical studies have made substantial achievements [4].

Cherenkov excited luminescence imaging (CELI) is a new modality of optical imaging [5], which utilizes the energy of Cherenkov photons [6] to excite fluorophores that emit fluorescence or phosphorescence photons. The Cherenkov photons can be generated either by radioactive nuclides [7], or by electron beams [8] and X-ray beams [9] delivered from medical linear accelerators (LINAC). In the latter case, CELI could be used to image the interaction between the distribution of delivered ionizing beams and the fluorophores. This indicates its potential for real-time and *in vivo* dosimetry, that is, to monitor the process of dose deposition to patients during the treatment delivery on-site.

In the practice of radiotherapy nowadays, although electron beams are effective in several specific diseases [10], most treatments are delivered using megavolt X-ray beams, from the perspective of clinical outcome [11]. Therefore, we believe that it is highly meaningful to develop CELI based radiation dosimetry methods for megavolt X-ray beams. However, the work is much challenging, not only because the electro-neutral X-ray beams induce Cherenkov radiation indirectly via secondary electrons but also due to the strong scattering and high penetration ability of the megavolt X-ray beams [12].

Cherenkov radiation is continuous in its spectrum, and the energy is the most intense in UV and blue range of the spectrum [13]. Although Cherenkov photons are generated in the whole volume where the criteria of Cherenkov radiation are met, only the superficial light could be visualized in a turbid medium, under the short-wavelength dominance. Thus, CELI could be used to convert the Cherenkov photons to photons with a desired wavelength via the photoluminescence effect. Many works have been done on megavolt X-ray beams to convert the energy to visible and near-infrared light [13–15]. However, to the best of our knowledge, no NIR-II CELI with megavolt X-ray beams has been reported. The major challenges include:

- the low sensitivity of the NIR-II detector arrays;
- the elevated level of noise induced by megavolt X-ray;

* Corresponding authors.
*E-mail addresses:* 13552661030@139.com (H. Wu), chli@pku.edu.cn (C. Li), yanye.lu@pku.edu.cn (Y. Lu).

https://doi.org/10.1016/j.optcom.2019.05.017
Received 1 March 2019; Received in revised form 9 April 2019; Accepted 12 May 2019
Available online 15 May 2019

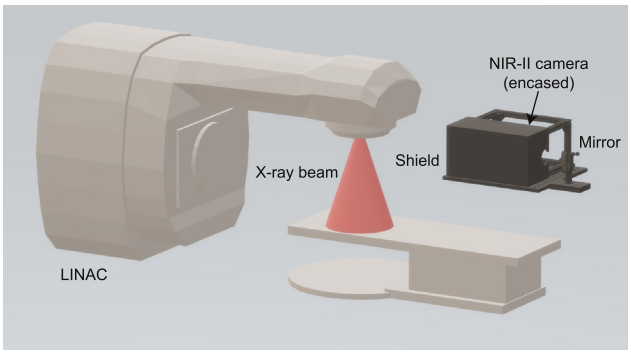


**Fig. 1.** The configuration of the LINAC and the imaging system.

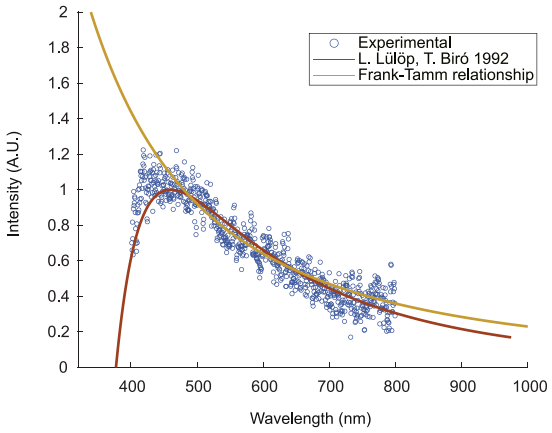


**Fig. 2.** The Cherenkov spectrum measured by the spectroscopic camera, and representative calculated spectra based on the Frank–Tamm and Lülöp–Biró models.

- the lack of fluorophores with super-large Stokes shift.

As the key originality and novelty, this study reports NIR-II CELI with megavolt X-ray beams delivered by radiotherapy LINAC, and explores its potential application as an *in vivo* and real-time dosimetric tool for radiotherapy.

In this work, the fluorescence signal excited by the megavolt X-ray beam from the LINAC was first reflected by a mirror, and captured by the NIR-II camera (NIRvana:640, Teledyne Princeton Instruments) encased in a lead shield. This design, as shown in Fig. 1, substantially decreases that the noise level induced by the X-ray beams, thus sufficient signal-to-noise ratio could be achieved even when the camera is close to the LINAC. The comparison of the pixel values of the dark-frame images acquired with and without the shield, as well as the one without the X-ray beams is provided in the supplementary data. This shows that, the design of the imaging system is crucial in the acquisition of the signal.

## 2. The selection of CELI fluorophore

For the NIR-II CELI, the choice of a fluorophore requires careful scrutiny. The overall relationship between the excitation light ($I_0$) and the emission light ($I_F$) could be written as:

$$I_F = \eta I_0 (1 - \Gamma) \tag{1}$$

where $\eta$ is the excitation efficiency, and the $\Gamma$ is the extinction component caused by absorption and scattering. Accordingly, several criteria should be met for an efficient CELI fluorophore:

- the excitation range should match the Cerenkov emission, thus a extra-large Stokes shift is required;
- the emission range should avoid the water molecular vibration band at around 1450 nm;
- the quantum yield should be high enough.
- preferably, the biocompatibility should allow *in vivo* applications.

The Cherenkov spectra of high energy photons or electrons are often estimated using the Frank–Tamm formula [16] in the UV to near infrared (NIR) range. The light intensity ($I_C$) generated by a charged particle is correlated with the wavelength ($\lambda$) by:

$$I_C = \frac{\pi e^2 \mu}{hc\lambda^2}\left(1 - \frac{c^2}{v^2 n(\lambda)^2}\right) \tag{2}$$

where $e$ is the elementary charge, $\mu$ is the permeability of the medium, $h$ is the Planck constant, $c$ is the speed of light, $v$ is the speed of the electron, and $n(\lambda)$ is the wavelength-dependent refractive index. However, this relationship becomes inaccurate in the short wavelength range [17]. More sophisticated relationships have been proposed by theoretical physicists, to better depict the spectral energy distribution of Cherenkov radiation [18,19].

The spectrum of Cherenkov radiation was measured on our system using a spectrometer (ImSpector V8E, Specim, Spectral Imaging Ltd.) equipped with an sCMOS camera (ORCA-Flash4.0 V2, Hamamatsu Photonics K.K.). The 10 MV X-ray beams were delivered to a water tank, and the spectra were taken with the integration time of 30 s. Due to the weak signal, the lower efficiency and the radiation noise, the spectra obtained were still noisy after applying a customized signal filter, as shown in Fig. 2. However, it is obvious that within the detection limits, the spectral energy distribution does not always follow the Frank–Tamm equation. Instead, we figured out a better description based on an equation proposed by Lülöp and Biró[20]. The Frank–Tamm equation and the Lülöp–Biró equation are proximate to each other in the longer wavelengths, however, the Lülöp–Biró equation depicts the cut-off threshold in the shorter wavelengths with a better accuracy. Although the measured distribution could not be fitted perfectly because either model overlooks factors such as the energy dispersion of the charged particles, the Lülöp–Biró equation captured the peak around 500 nm. Precised knowledge of the spectral peak is especially important for CELI, where the intensity distribution should match the excitation spectrum as much as possible.

There are only a limited types of fluorophores to choose from for NIR-II photoluminescence applications. In conventional *in vivo* imaging, the excitation light is favorably in longer wavelength such as the conventional NIR window [21], as in most organic dyes [22] and rare earth nanoparticles [23]. After screening several classes of fluorescence materials and molecules, we found that the PbS quantum dots (QDs) is a promising candidate as an NIR-II CELI fluorophore [24]. First, the excitation spectrum of the PbS QDs overlaps almost perfectly with the Cherenkov emission spectrum, thus the QDs could fully utilize the Cherenkov photon energy. Second, the Stokes shift of the PbS QDs is very large, thus the QDs could easily transfer the Cherenkov photon energy to the favorable NIR-II range. Finally, the emission peak of the PbS QDs could be easily adjusted with different synthetic parameters, to avoid overlapping with the absorption peak of water, which poses a negative impact on the intensity of the observed signal. Fig. 3 shows the excitation and emission spectra of the QD chosen, and a calculated Cherenkov emission spectrum, as well as a water absorption spectrum [25]. It suggests that this particular type of QD meets all the criteria for CELI fluorophores.

## 3. Phantom study

Water phantoms were first used to demonstrate the NIR-II CELI of megavolt X-ray beams. As the megavolt X-ray CELI technique in visible to near-infrared (Vis-NIR) range is already studied, we used it to compare with CELI in NIR-II range. The fluorophore for Vis-NIR CELI

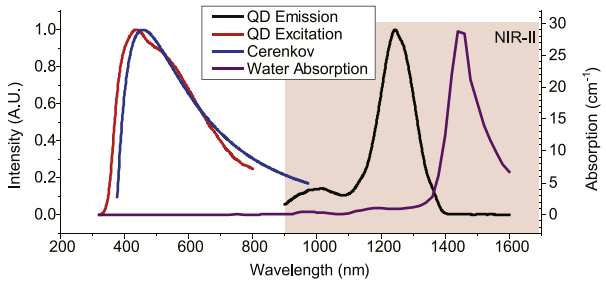


**Fig. 3.** The Cherenkov spectrum, the excitation and emission spectrum of the quantum dots, and the absorption spectrum of water [25].

is a solution of an organic dye, coumarin 6, whose photoluminescence spectra are shown in the supplementary data. The QD colloid and the organic dye solution were filled in glass vials, respectively. The vials were sealed and placed juxtaposed on metal holders in a water tank made by Super White glass. Then, a beam of 10 MV X-ray was delivered by the LINAC, whose field covered both vials, as shown in Fig. 4(c). An NIR-II camera equipped with a 1050 nm long pass filter and a Vis-NIR CCD camera (Andor iKon-M 934, Oxford Instruments plc) were used to capture the emitted photon. The images acquired were processed to remove the Cherenkov emission background, and were merged with the white light image of the tank, as shown in Fig. 4(a) for Vis-NIR CELI and in Fig. 4(b) for NIR-II CELI.

The signal of the coumarin 6 solution was captured by the Vis-NIR camera, and in the meantime, the corresponding signal from the QD was captured by the NIR-II camera. Due to the differential wavelength sensitivity of the detectors, neither camera captured any signal from the other vial of fluorophore. This experiment shows that the NIR-II CELI induced by megavolt X-beams can be visualized specifically by the NIR-II imaging system.

One of the major superiority of megavolt X-ray beams relative to high energy electron beams is the deeper penetration depth in tissues. The penetration ability of the X-ray beams is demonstrate by the fact that the percentage depth dose curve of the X-ray beams extends to a range much deeper than that of the electron beams, as shown in the supplementary data. An experiment was conducted on a water phantom to demonstrate the penetrative effect on NIR-II CELI. A larger water tank was used, which was filled with water of 300 mm in height. A glass vial of QDs was placed at different positions depths (50 mm, 150 mm and 250 mm) under water. A 10 MV X-ray beam was delivered in each case and the emission signals were collected by the NIR-II camera, as shown in Fig. 5. This experiment demonstrated that the NIR-II CELI signal could be visualized from various depths inside the water tank, owing to the superior penetration ability of the X-ray beams.

To further explore the possible application of CELI, an experiment exploring the condition of CELI was conducted. The QD, sealed in the vial, was placed in a water tank. A beam of 10 MV X-ray was delivered, and the CELI signal was monitored by the NIR-II camera. The field was set in different positions, so that the QD was first off the field, as shown in Fig. 6(a, b); then the QD was at the edge of the field, as shown in Fig. 6(c, d); and finally, the QD was in the center of the field, as shown in Fig. 6(e, f).

The two key factors of CELI are the ionizing radiation and the fluorophore, and the luminescence photons only emit when the two factors combine. In this experiment, the CELI signal could only be observed when the QD is in within the field. When the QD was at the edge of the field, it fell in the penumbra region where the Cherenkov intensity was not high enough to generate fluorescence photons. This effect shows that CELI could be a qualitative tool to study the delivery of radiation dose to a predetermined region.

## 4. Animal study

Animal experiments were conducted to demonstrate the potential applications of CELI. The animal procedures were approved by the Institutional Animal Care and Use Committee of Peking University. First,

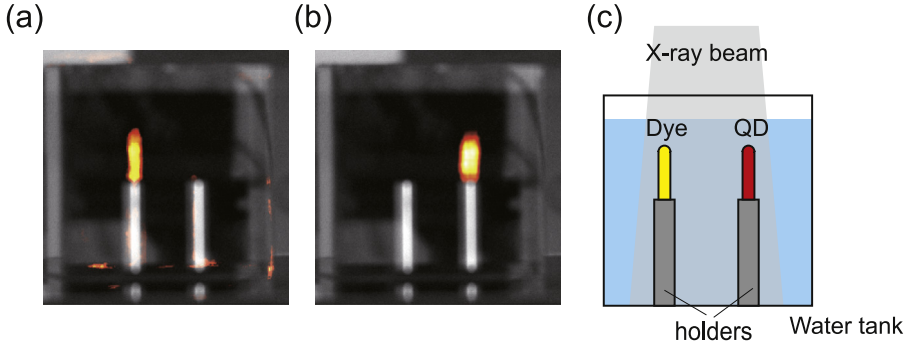


**Fig. 4.** The comparison between Vis-NIR (a) and NIR-II (b) Cherenkov signal, and a schematic drawing showing the configuration of the phantom (c).

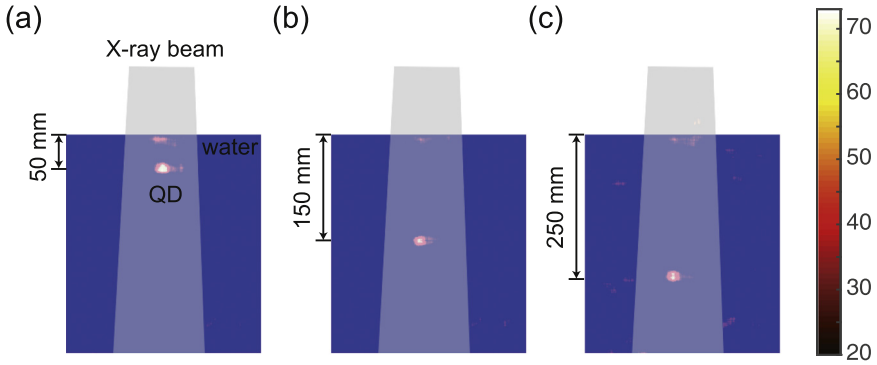


**Fig. 5.** The CELI of the quantum dots at a depth of 50 mm (a), 150 mm (b) and 250 mm (c).

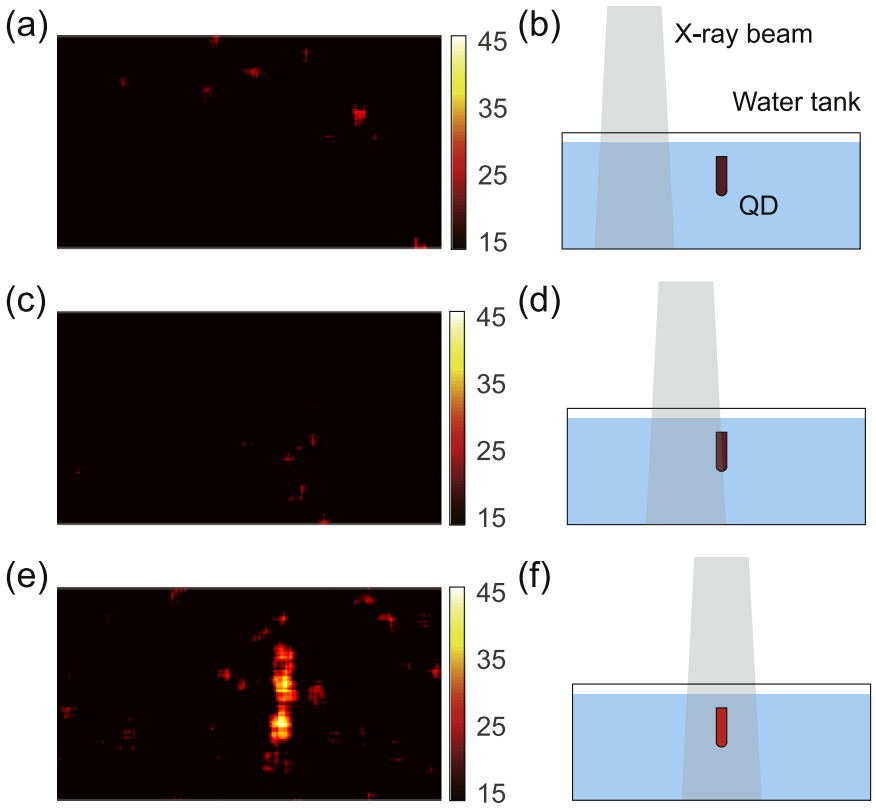


**Fig. 6.** The QD could only be illuminated when it is within the field. There is no signal (a,c) when the QD is off the field (b) or at the edge of the field (d), and visible (e) when in the field (f).

100 μL of the QD colloid (10 nmol/mL) was injected subcutaneously near the hind limb of an anesthetized BALB/c nude mouse. A 10 MV X-ray beam was delivered covering the whole mouse, and the CELI was obtained as shown in Fig. 7(a). Then, another 100 μL of the QD colloid was injected subcutaneously near the front limb of the same animal, and the CELI was obtained as shown in Fig. 7(b). Then, the field was shrunk to cover only the anterior part of the same animal, and the CELI was obtained again as shown in Fig. 7(c). The corresponding schematic diagrams are shown in Fig. 7(d–f).

This experiments shows that the NIR-II CELI could be a tool to monitor dose delivery intuitively during radiotherapy. The QD could mark the regions to deliver the radiation (planning target volume) or to protect from the radiation (planned organ at risk volume). If the positions of the QD are precise, the delivery of radiation to specific regions could be visualized with the NIR-II camera simultaneously. Combined with targeted delivery, CELI could even be used as a theragnostic tool.

Finally, a BALB/c mouse bearing a human HCT116 tumor was anesthetized, and 100 μL of QD was injected intratumorally. The CELI of this mouse was conducted. Fig. 7(g) show the Cherenkov emission obtained before the injection of the QD. Fig. 7(h) shows the corresponding CELI result. Unlike the CELI, which shows the combined effect of the radiation and the fluorophore, Cherenkov imaging only shows the distribution of radiation field.

Due to the penetrative ability of X-ray beams, and the imaging ability of the NIR-II light, NIR-II CELI induced by X-ray beams could be used to visualize signals from deeper tissues. Apart from subcutaneously injected QD, QD inside the tumor could also be visualized with NIR-II CELI induced by X-ray beams. Admittedly, the contrast between the signal and the Cherenkov background is smaller in the intratumoral situation, as shown in Fig. 7(i). This is because the thicker layer of tissue absorbed some of the fluorescence emission. This deep-tissue imaging application demonstrates the practical aspect of CELI.

## 5. Conclusion

In this report, we demonstrated the feasibility of CELI induced by megavolt X-ray beams in the NIR-II range with our customized imaging system, which effectively reduced the noise enabling the acquisition of CELI signals. The Cherenkov spectrum was first measured by a spectroscopic camera, and a specific QD for NIR-II CELI was chosen according to the spectral information. CELI was then realized, and it could be captured at different depth in a water tank. As CELI is a binary imaging method, it was revealed that the CELI signal could only be visible if the QD is within the radiation field. Animal experiments verified that CELI is capable of differentiating volumes where radiation dose is delivered. Finally, NIR-II CELI induced by X-ray beams was visualized from inside a tumor.

CELI provides a solution to the problem of deep-tissue imaging. In conventional NIR-II photoluminescence imaging, the propagation of the excitation light inside the tissue must also be optimized to fully exploit the benefit of the NIR-II imaging. Although CELI also utilizes the photoluminescence effect, the excitation light is generated *in situ*, and is determined by the penetrative ability of the charged particles. As long as the energy of the particle is high enough, the depth of imaging could be extended. However, the major problem is in the instruments. The performance of the current InGaAs detectors is far from satisfactory, and no time-gating technology [26] is available on this types of cameras. There is still room for better elimination of the X-ray artifacts, especially if silicon-based NIR-II detectors could be developed [27].

## Acknowledgments

This work is supported by the National Key Instrumentation Development Project of China (2013YQ030651), National Natural Science Foundation of China (NSFC) (81421004, 61571262, 11575095, 11505012), Natural Science Foundation of Beijing Municipality (No.

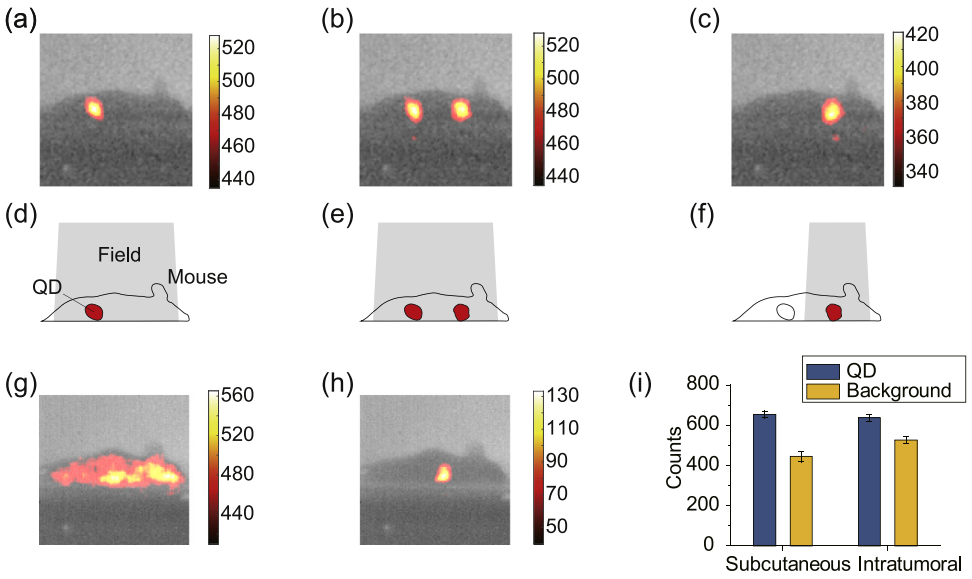


**Fig. 7.** The NIR-II CELI and Cherenkov imaging of a mouse and the corresponding geometric configurations where the QD is injected (a)–(f) subcutaneously or (h)intratumorally. In (a) and (d) there is one spot of QD and the field covers the whole body; in (b) and (e) there are two spots of QD and the field covers the whole body; in (c) and (f) there are two spots of QD and the field covers only one of the spots. (g) shows the NIR-II Cherenkov background of a mouse and in (h) the QD is injected intratumorally into the same animal. (i) is a comparison between the CELI signal and the background signal under two representative scenarios.

1184014, 1174016), China Postdoctoral Science Foundation (No. 2017-M620542), and Capital's Funds for Health Improvement and Research (No. 2018-4-1027).

## Appendix A. Supplementary data

Supplementary material related to this article can be found online at https://doi.org/10.1016/j.optcom.2019.05.017.

## References

[1] A. Smith, M. Mancini, S. Nie, Bioimaging: Second window for *in vivo* imaging, Nature Nanotechnol. 4 (11) (2009) 710–711.
[2] G. Hong, A. Antaris, H. Dai, Near-infrared fluorophores for biomedical imaging, Nat. Biomed. Eng. 1 (1) (2017) 0010.
[3] F. Ding, Y. Zhan, X. Lu, Y. Sun, Recent advances in near-infrared II fluorophores for multifunctional biomedical imaging, Chem. Sci. 9 (19) (2018) 4370–4380.
[4] K. Welsher, Z. Liu, S. Sherlock, J. Robinson, Z. Chen, D. Daranciang, H. Dai, A route to brightly fluorescent carbon nanotubes for near-infrared imaging in mice, Nature Nanotechnol. 4 (11) (2009) 773–780.
[5] J. Axelsson, S.C. Davis, D.J. Gladstone, B.W. Pogue, Cerenkov emission induced by external beam radiation stimulates molecular fluorescence, Med. Phys. 38 (7) (2011) 4127–4132.
[6] K. Tanha, A.M. Pashazadeh, B.W. Pogue, Review of biomedical Čerenkov luminescence imaging applications, Biomed. Opt. Express 6 (8) (2015) 3053–3065.
[7] R. Dothager, R. Goiffon, E. Jackson, S. Harpstrite, D. Piwnica-Worms, Cerenkov radiation energy transfer (CRET) imaging: A novel method for optical imaging of PET isotopes in biological systems, PLoS ONE 5 (10) (2010) e13300.
[8] X. Cao, S. Jiang, M. Jia, J. Gunn, T. Miao, S. Davis, P. Bruza, B. Pogue, Cherenkov excited short-wavelength infrared fluorescence imaging *in vivo* with external beam radiation, J. Biomed. Opt. 24 (5) (2019) 051405.
[9] R. Zhang, A. D'souza, J. Gunn, T. Esipova, S. Vinogradov, A. Glaser, L. Jarvis, D. Gladstone, B. Pogue, Cherenkov-excited luminescence scanned imaging., Opt. Lett. 40 (5) (2015) 827–830.
[10] C. Griep, J. Davelaar, A.N. Scholten, A. Chin, J.-W.H. Leer, Electron beam therapy is not inferior to superficial X-ray therapy in the treatment of skin Carcinoma, Int. J. Radiat. Oncol. Biol. Phys. 32 (5) (1995) 1347–1350.
[11] C. DesRosiers, V. Moskvin, A.F. Bielajew, L. Papiez, 150-250 MeV electron beams in radiation therapy, Phys. Med. Biol. 45 (7) (2000) 1781–1805.
[12] X. Cao, S. Jiang, M. Jia, J. Gunn, T. Miao, S.C. Davis, P. Bruza, B.W. Pogue, Observation of short wavelength infrared (SWIR) cherenkov emission, Opt. Lett. 43 (16) (2018) 3854–3857.
[13] E. LaRochelle, J. Shell, J. Gunn, S. Davis, B. Pogue, Signal intensity analysis and optimization for in vivo imaging of Cherenkov and excited luminescence, Phys. Med. Biol. 63 (8) (2018) 085019.
[14] M.J. Jia, P. Bruza, L.A. Jarvis, D.J. Gladstone, B.W. Pogue, Multi-beam scan analysis with a clinical LINAC for high resolution Cherenkov-excited molecular luminescence imaging in tissue, Biomed. Opt. Express 9 (9) (2018) 4217–4234.
[15] S.R. Ahmed, J.M. Jia, P. Bruza, S. Vinogradov, S. Jiang, D.J. Gladstone, L.A. Jarvis, B.W. Pogue, Radiotherapy-induced Cherenkov luminescence imaging in a human body phantom, J. Biomed. Opt. 23 (3) (2018) 030504.
[16] I. Frank, I. Tamm, Coherent visible radiation of fast electrons passing through matter, Dokl. Akad. Nauk SSSR 14 (1937) 109–114.
[17] G. Collins, V. Reiling, Čerenkov Radiation, Phys. Rev. 54 (7) (1938) 499–503.
[18] C. Kremers, D.N. Chigrin, J. Kroha, Theory of Cherenkov radiation in periodic dielectric media: Emission spectrum, Phys. Rev. A 79 (1) (2009) 013829.
[19] I. Carusotto, M. Artoni, G.C. La Rocca, F. Bassani, Slow group velocity and Cherenkov radiation, Phys. Rev. Lett. 87 (2001) 064801.
[20] L. Fülöp, T. Biró, Cherenkov radiation spectrum, Internat. J. Theoret. Phys. 31 (1) (1992) 61–74.
[21] E. Hemmer, A. Benayas, F. Légaré, F. Vetrone, Exploiting the biological windows: current perspectives on fluorescent bioprobes emitting above 1000 nm, Nanoscale Horiz. 1 (3) (2016) 168–184.
[22] A. Antaris, H. Chen, K. Cheng, Y. Sun, G. Hong, C. Qu, S. Diao, Z. Deng, X. Hu, B. Zhang, X. Zhang, O.K. Yaghi, Z.R. Alamparambil, X. Hong, Z. Cheng, H. Dai, A small-molecule dye for NIR-II imaging, Nature Mater. 15 (2) (2015) 235–242.
[23] Y. Zhong, Z. Ma, S. Zhu, J. Yue, M. Zhang, A.L. Antaris, J. Yuan, R. Cui, H. Wan, Y. Zhou, W. Wang, N.F. Huang, J. Luo, Z. Hu, H. Dai, Boosting the down-shifting luminescence of rare-earth nanocrystals for biological imaging beyond 1500 nm, Nature Commun. 8 (1) (2017) 737–744.
[24] M. Zhang, J. Yue, R. Cui, Z. Ma, H. Wan, F. Wang, S. Zhu, Y. Zhou, Y. Kuang, Y. Zhong, D.-W. Pang, H. Dai, Bright quantum dots emitting at ~1600nm in the NIR-IIb window for deep tissue fluorescence imaging, Proc. Natl. Acad. Sci. 115 (26) (2018) 6590–6595.
[25] G.M. Hale, M.R. Querry, Optical constants of water in the 200-nm to 200-μm wavelength region, Appl. Opt. 12 (3) (1973) 555–563.
[26] J. Andreozzi, R. Zhang, A. Glaser, L. Jarvis, B. Pogue, D. Gladstone, CaMera selection for real–time *in vivo* radiation treatment verification systems using Cherenkov imaging, Med. Phys. 42 (2) (2015) 994–1004.
[27] S. Goossens, G. Navickaite, C. Monasterio, S. Gupta, J. Piqueras, R. Pérez, G. Burwell, I. Nikitskiy, T. Lasanta, T. Galán, E. Puma, A. Centeno, A. Pesquera, A. Zurutuza, G. Konstantatos, F. Koppens, Broadband image sensor array based on graphene-CMOS integration, Nat. Photonics 11 (6) (2017) 366–371.